

EVOLUTION SINCE Z=1 OF THE MORPHOLOGY–DENSITY RELATION FOR GALAXIES

GRAHAM P. SMITH,^{1,2} TOMMASO TREU,^{1,3} RICHARD S. ELLIS,¹
SEAN M. MORAN,¹ AND ALAN DRESSLER⁴

Draft version October 29, 2018

ABSTRACT

We measure the morphology–density relation of galaxies at $z=1$ across the full three orders of magnitude in projected galaxy density available in low–redshift studies. Our study adopts techniques that are comparable with those applied at lower redshifts, allowing a direct investigation of how the morphological segregation of galaxies has evolved over the last 8 Gyr. Although the morphology–density relation, as described by the fraction of early–type (E+S0) galaxies, was in place at $z=1$, its form differs from that observed at both $z=0$ and $z=0.5$. In the highest density regions the early–type fraction has increased steadily with time from $f_{E+S0}=0.7\pm 0.1$ at $z=1$ to $f_{E+S0}=0.9\pm 0.1$ at the present epoch. However, in intermediate density regions corresponding to groups and the accretion regions of rich clusters, significant evolution appears to begin only after $z=0.5$. Finally, at the lowest densities, no evolution is observed for the early type fraction of field galaxies which remains constant at $f_{E+S0}=0.4\pm 0.1$ at all epochs. We examine a simple picture consistent with these observations where the early–type population at $z=1$ is comprised largely of elliptical galaxies. Subsequent evolution in both intermediate and dense regions is attributed to the transformation of spirals into lenticulars. Further progress in verifying our hypothesis may be achieved through distinguishing ellipticals and lenticulars at these redshifts through resolved dynamical studies of representative systems.

Subject headings: galaxies: clusters: general — galaxies: formation — galaxies: evolution — galaxies: structure

1. INTRODUCTION

In the local universe the fraction of galaxies with elliptical and lenticular (i.e. early–type) morphologies is higher in clusters of galaxies than in less dense environments (Hubble 1926; Oemler 1974; Melnick & Sargent 1977; Dressler 1980). To first order, this morphology–density relation appears to be a universal characteristic of galaxy populations (e.g. Postman & Geller 1984; Helsdon & Ponman 2003). In quantitative terms, morphological fractions correlate over three orders of magnitude in projected galaxy density (Σ), thereby linking the properties of cluster galaxies ($\Sigma \simeq 1000 \text{Mpc}^{-2}$) with those of the field galaxy population ($\Sigma \lesssim 10 \text{Mpc}^{-2}$) (Dressler 1980).

The morphological segregation of galaxies is a generic prediction of cold dark matter simulations of large scale structure formation (Frenk et al. 1985, 1988), and more recent semi–analytic galaxy formation models (Kauffmann 1995; Baugh et al. 1996; Benson et al. 2001; Diaferio et al. 2001). In that context, the observed morphology–density relation is interpreted as the combination of two mechanisms. Firstly, the local density of galaxies and dark matter is a proxy for the epoch of initial collapse of a given structure; the most massive structures at any epoch represent the earliest that collapsed. Secondly, interactions between galaxies, dark matter and the intra–cluster medium (i.e. environmental processes) are likely to transform in–falling field galaxies from gas–rich spirals to gas–poor lenticular galaxies. The exact balance between these two mechanisms (i.e. nature versus nurture) and the detailed physics of the environmental processes have yet to be identified unambiguously, and are the focus of much ongoing re-

search (e.g. Balogh et al. 2001; Kodama & Smail 2001; Treu et al. 2003).

An important element of investigating the physics of morphological transformation is to trace the cosmic evolution of the morphology–density relation over the full range of projected density available locally. The timescales on which the relation evolves in different density regimes will hold important clues to the physical processes responsible. To that end, Dressler et al. (1997) used high–resolution imaging with the *Hubble Space Telescope (HST)* to measure the morphology–density relation in the core regions of a sample of rich clusters at $z \simeq 0.5$. Dressler et al. found that the fraction of lenticular galaxies in clusters declined by a factor of 2–3 between $z=0$ and $z=0.5$ and this evolution was accompanied by a corresponding increase in the fraction of star–forming spirals (see also Andreon 1998; Couch et al. 1998; Fasano et al. 2000; Treu et al. 2003).

At higher redshifts, the distinction between elliptical and lenticular morphologies becomes increasingly difficult to draw (Smail et al. 1997; Fabricant et al. 2000). Nevertheless, several authors have measured the total early–type fraction f_{E+S0} in individual clusters at $z \simeq 1$ (e.g. van Dokkum et al. 2000, 2001; Lubin et al. 2002). These authors find $f_{E+S0}=0.5$ in clusters at $z \simeq 1$, i.e. a smaller fraction than that found in the densest environments at $z=0$. However, as van Dokkum & Franx (2001) caution, these estimates are preliminary because they are based on a very small number of clusters.

In this paper we measure the morphology–density relation at $z=1$ across the full three orders of magnitude in galaxy density spanned in local samples. We compare our results with those obtained at lower and intermediate redshifts (Dressler 1980; Dressler et al. 1997; Treu et al. 2003) and thus chart, for the first time, the form of the morphology–density relation over a cosmologically significant time interval (~ 8 Gyr).

A plan of the paper follows. In §2 we develop a strategy for measuring the morphology–density relation at $z=1$ and sum-

¹ California Institute of Technology, Department of Astronomy, Mail Code 105–24, Pasadena, CA 91125, USA.

² Email: gps@astro.caltech.edu

³ Hubble Fellow; Department of Physics and Astronomy, University of California at Los Angeles, Los Angeles, CA 90095, USA.

⁴ The Observatories of the Carnegie Institute of Washington, 813 Santa Barbara Street, Pasadena, CA 91101, USA.

marize the data used for this purpose. Then in §3 we describe the analysis, focusing separately on high- and low-density environments. The main results, the morphology–density relation at $z=1$ and its evolution to the present–day are presented in §4. In §5 we discuss a possible interpretation, including how it relates to previous measurements of f_{E+S0} in high–redshift clusters. We summarize our conclusions in §6. We parameterize the Hubble expansion as $h=H_0/100\text{kms}^{-1}\text{Mpc}^{-1}=0.65$, and adopt the currently favored values of $\Omega_M=0.3$ and $\Omega_\Lambda=0.7$ when our analysis requires us to make distance estimates. In this cosmology $1''\equiv 8.63\text{kpc}$ physical size at $z=1$. Unless otherwise stated, all error bars are stated at $1-\sigma$ significance. All magnitudes are quoted in the Vega system.

2. DATA

2.1. Strategy

The primary aims of this paper are to measure the morphology–density relation at $z\approx 1$ and to identify broad evolutionary trends by comparing our measurements with those at $z\approx 0$ (Dressler 1980) and $z\approx 0.5$ (Dressler et al. 1997; Treu et al. 2003). To facilitate this comparison, we adopt the same analysis methods used in the lower redshift studies, and provide two measurements for carefully selected galaxy populations at $z=1$ which form the basis of our analysis. The projected number density (Σ) of galaxies down to $M_V \leq M_V^* + 1$ allows us to measure the projected density, $\Sigma \equiv 10/A$, where A is the solid angle within which the ten nearest neighbors are found (see §3 for more details). We also morphologically classify the galaxies in the various $z=1$ samples. Both Σ and morphologies need to be derived in a homogeneous fashion across the full range in projected density: $1 < \Sigma < 1000 \text{Mpc}^{-2}$.

Dressler et al. (1997) used *HST* observations of 10 optically–selected clusters to measure the morphology–density relation for cluster galaxies at $z\approx 0.5$, i.e. $50 \lesssim \Sigma \lesssim 1000 \text{Mpc}^{-2}$. Treu et al.’s (2003) wide–field (out to a projected cluster–centric radius of 5 Mpc) study of Cl 0024 extends Dressler et al.’s results out to field environments $\Sigma \approx 1 \text{Mpc}^{-2}$ for one cluster. To extend this body of work to $z=1$ we sought *HST* imaging of a similar sized sample of clusters at $z\approx 1$. A search of the *HST* archive for WFPC2 observations of clusters at $0.75 \leq z \leq 1.25$ through the F814W filter (i.e. a reasonable match to rest–frame V –band) yielded a sample of six clusters for which thirteen individual WFPC2 pointings are available (Table 1).

To measure the morphological fractions at $\Sigma \approx 1 \text{Mpc}^{-2}$, we complement these cluster data with a sample of field galaxies. Prior to large–scale redshift surveys of galaxies at $z=1$ in regions where *HST* data is available (e.g. Davis et al. 2002; Le Fèvre et al. 2003), we necessarily rely on photometric redshift estimates. We therefore selected a field for which a deep photometric dataset with broad wavelength coverage and *HST* imaging through the F814W filter is available. The mosaiced *HST* field containing the rich cluster Cl 0024 ($z=0.395$) is well–matched to this purpose as the bulk of the faint population viewed is not associated with the foreground cluster. Ground–based *BVRJK*–photometry, plus F814W *HST*/WFPC2 imaging are available (Kneib et al. 2003) and the projected physical extent is $\sim 170 \text{Mpc}^2$ at $z=1$, corresponding to a volume of $5 \times 10^5 \text{Mpc}^3$ when integrated over a redshift interval $0.75 \leq z \leq 1.25$. Extensive spectroscopic studies of this field (Czoske et al. 2001; Treu et al. 2003; Moran et al. 2004, in prep.) provide several hundred spectroscopic red-

TABLE 1
SUMMARY OF *HST* DATA

	Redshift	$T_{\text{exp}}(\text{ks})$	Pointings	PID	Reference
RCS 0224–0002	0.77	13.2	1	9135	<i>a</i>
RXJ 0848+4453	1.27	28.0	1	6812	<i>b</i>
MS 1054–0321	0.83	6.5	6	7372	<i>c</i>
MS 1137+6624	0.78	15.0	1	5987	
Cl 1325+3009	0.76	19.0	1	6581	<i>d</i>
Cl 1604+4304	0.90	19.0	3	8560	<i>e</i>
Cl 0024+1654	0.395	4.4	38	8559	<i>f</i>
Cl 0024+1654	0.395	18.0	1	5453	

^a Gladders et al. (2002)

^b van Dokkum et al. (2001)

^c van Dokkum et al. (2000)

^d Lubin, Oke & Postman (2002)

^e Postman, Lubin & Oke (2001) – these data include Cl 1604+4321.

^f Treu et al. (2003) – these data are used to characterize the $z\approx 1$ galaxy population, and not the galaxies that inhabit the foreground cluster at $z=0.4$.

shifts which are useful in calibrating photometric redshift estimates based on the *BVRJK*–band photometry (see §3.1.2).

In comparing morphological fractions at different redshifts, in addition to k –corrections and adopting a fixed luminosity limit of $M_V^* + 1$, the question of luminosity evolution in the population needs to be considered. Interpolating between the redshift–dependent B – and R –band luminosity functions we estimate that evolution of M_V^* between $z=1$ and $z=0$ is 1 mag (Brown et al. 2001; Chen et al. 2003; Norberg et al. 2002; Poli et al. 2003). Although there is some uncertainty in this estimate, we conclude it is better to apply this adjustment rather than to ignore the effect altogether. We therefore subtract 1 mag of evolution from M_V^* at $z=0$ (Brown et al. 2001), to define a luminosity limit 1 mag fainter than M_V^* at $z=1$, i.e. $M_V \leq -21.2$.

2.2. Space–based Observations

A wide–field sparse–sampled *HST*/WFPC2⁵ mosaic of Cl 0024 ($z=0.395$) was acquired during Cycle 8 (PI: R.S. Ellis, GO:8559), comprising 38 independent pointings observed through the F814W filter for two orbits each. Treu et al. (2003) describe the reduction of these data; here we summarize key details of the reduced data: the pixel–scale is $0''.05$ after drizzling; the estimated 80% completeness limit is $I_{814} \approx 25$; the total combined field of view of the 39 pointings (including the cluster center – e.g. Smail et al. 1997) is 0.05deg^2 , excluding the PC chip from each pointing. The primary motivation of these observations was a panoramic study of the rich cluster Cl 0024 (Treu et al. 2003; Kneib et al. 2003). However, as discussed, these data provide morphological information on a large sample of field galaxies at $z\approx 1$ (§3.2). The limiting magnitude of these data corresponds to $M_V \approx -20$ at $z=1$, i.e. sufficiently deep to provide early/late–type morphological classification in a manner consistent with that of earlier work (see §3.2 for more details of the classification process, including estimation of uncertainties).

⁵ This paper is based on observations with the NASA/ESA *Hubble Space Telescope*, obtained at the Space Telescope Science Institute (STScI), which is operated by the Association of Universities for Research in Astronomy, Inc., under NASA contract NAS5–26555.

TABLE 2
SUMMARY OF GROUND-BASED DATA

Filter	Telescope/Instrument	$3\text{-}\sigma$ Limit	FWHM(")
<i>B</i>	CFH12k	27.8	0.92 ± 0.06
<i>V</i>	CFH12k	26.9	0.79 ± 0.12
<i>R</i>	CFH12k	26.6	0.88 ± 0.09
<i>I</i>	CFH12k	25.9	0.77 ± 0.09
<i>J</i>	Hale/WIRC	22.0	0.95 ± 0.11
<i>K</i>	Hale/WIRC	20.4	0.93 ± 0.10

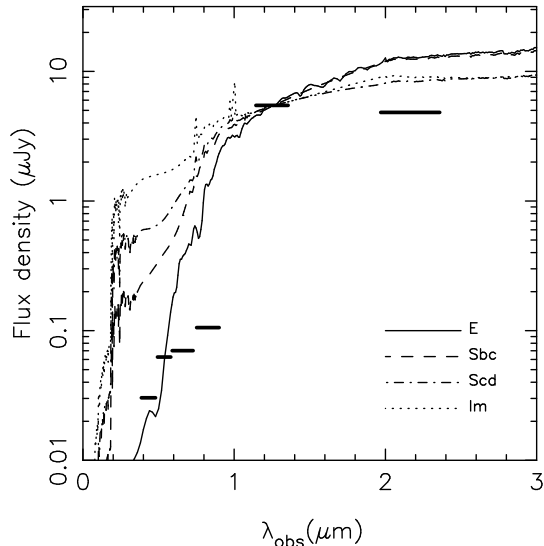


FIG. 1.— Observed detection limits for ground-based imaging of the Cl0024 field, ($3\text{-}\sigma$ significance, except for the *J*-band, shown at $5\text{-}\sigma$). Coleman, Wu & Weedman spectral templates have been redshifted to $z=1$ and normalized to the *V*-band luminosity of a galaxy at $z=1$ with $M_V = M_V^* + 1 = -21.2$ (see §2.1 for details). Our ground-based data is shown to be sufficiently deep across the broad wavelength range to achieve accurate photometric redshifts for all spectral types (see §2.3 for further details).

The high-redshift cluster data (Table 1) were reduced using the WFIXUP, WMOSAIC, IMALIGN, IMCOMBINE and COSMICRAYS tasks in IRAF⁶. The reduced frames have a pixel-scale of $0''.1$ and the mean FWHM of stellar profiles is $0''.17$. As this pixel scale is twice that of the field-galaxy data described above, we block-averaged the field data for the purpose of morphological classification. Although this results in a slight under-sampling of the WFPC2 point-spread-function, the larger pixels assist in the identification of faint morphological features. Although these cluster data are deeper than the corresponding field images (see Table 1), both are sufficiently deep for the morphological classification exercise (§3.2).

2.3. Ground-based Observations

⁶ IRAF is distributed by the National Optical Astronomy Observatories, which are operated by the Association of Universities for Research in Astronomy, Inc., under cooperative agreement with the National Science Foundation.

Panoramic optical data of Cl0024 were acquired with the 3.6-m Canada France Hawaii Telescope⁷ using the CFH12k camera (Cuillandre et al. 2000) through the *BVRI* filters. These data are described by Czoske (2002) and Treu et al. (2003). The sensitivity limit and image quality achieved in each passband is given in Table 2. The optical data are complemented by wide-field *J*- and *K_s*-band (hereafter *K*-band) imaging obtained with the WIRC camera (Wilson et al. 2002) at the Hale 200" telescope⁸ on 2002, October 29–30. These near-infrared (NIR) observations comprise a 3×3 mosaic of WIRC pointings, providing a contiguous observed area of $\sim 26'\times 26'$ centered on the cluster. Further details of these observations and the data reduction are described by Kneib et al. (2003). Here, we note that independent checks on the absolute photometric calibration using unsaturated sources in the 2MASS point-source and extended-source catalogs⁹, together with examination of the sources that fall in the overlap regions between the nine pointings confirm that the absolute and relative calibration of both the *J*- and *K*-band data are accurate to 10%. We incorporate these uncertainties into the spectral template fitting described in §3. All of the ground-based data were registered onto Czoske et al.'s (2001) astrometric grid, which is accurate to $\lesssim 0.2''$.

An important question is whether the depth of this multi-passband data is adequate for reliable photometric redshift studies at $z=1$ described in §3.1.2. We compare the depth of the ground-based data as a function of wavelength to spectral templates derived from observations of local galaxies (Coleman, Wu & Weedman 1980 – CWW). We redshifted the CWW templates to $z=1$ and normalized them to $M_V = -21.2$ (see §2.1), and compared them with detection limits listed in Table 2 (note that the *J*-band detection limit is shown at $5\text{-}\sigma$ significance because this is the detection filter adopted in §3.1.2). Fig. 1 confirms that the ground-based data are sufficiently deep to provide strong signal-to-noise detections across the full wavelength range from *B*- to *K*-bands for all but the reddest spectral types. The slight short-fall in sensitivity in the bluest filters is not a significant concern because we have ignored spectral evolution when constructing Fig. 1. Indeed, only 3% of the galaxies at $z\approx 1$ in the final photometric redshift catalog are undetected in the *B*-band.

3. ANALYSIS

In this section we describe how we construct samples of cluster and field galaxies at $z=1$ and measure the projected density, Σ , at the location of each galaxy (§3.1). In §3.2, we describe the morphological classification.

3.1. Measuring the Local Galaxy Density

3.1.1. High Density Environments

We begin with the high density environments, using the pointed WFPC2 observations of high redshift clusters (Table 1). We analyzed each WFPC2 frame with SExtractor

⁷ The Canada-France-Hawaii Telescope (CFHT) is operated by the National Research Council of Canada, l'Institut National des Science de l'Univers of the Centre National de la Recherche Scientifique of France and the University of Hawaii.

⁸ The Hale Telescope at Palomar Observatory is owned and operated by the California Institute of Technology.

⁹ This paper makes use of data products from the Two Micron All Sky Survey (2MASS), which is a joint project of the University of Massachusetts and the Infrared Processing and Analysis Center/California of Technology, funded by the National Aeronautics and Space Administration and the National Science Foundation.

(Bertin & Arnouts 1996), and adopted `MAG_AUTO` as an estimate of the total I_{814} –band magnitude of each source. Assuming all the detected sources are at the cluster redshifts (we discuss corrections for contamination by field galaxies below), the total I_{814} –band magnitudes were converted into the rest–frame V –band using correction terms derived from synthetic spectral templates for a representative range of stellar population ages (2–8 Gyr – see Treu et al. (2001, 2003) for more details). We estimate that this step introduces an uncertainty of $\lesssim 0.1$ mag in the estimated M_V luminosity. We then select all galaxies with $M_V \leq -21.2$ (i.e. the limit defined in §2.1).

The projected number density was calculated for each of the 957 galaxies in the resulting catalog following the precepts introduced by Dressler (1980). For each galaxy we counted the ten nearest neighbors and divided by the rectangular area enclosed. The median value of Σ computed in this manner is $\Sigma \simeq 400 \text{ Mpc}^{-2}$; $\sim 80\%$ of the galaxies have $\Sigma \gtrsim 200 \text{ Mpc}^{-2}$. Contamination arising from the projection of field galaxies at lower and higher redshifts along the line–of–sight was corrected using Postman et al.’s (1998) I –band number counts. Given the broad bins in Σ required to achieve reasonable signal–to–noise (Fig. 3), uncertainties arising from this correction do not significantly affect the final cluster–based results.

3.1.2. Low Density Environments

We now turn to the low density environments, as probed by the wide–field observations of C10024. The WIRC J –band mosaic is of key importance here since it provides a reasonable match to rest–frame V –band at $0.75 \leq z \leq 1.25$. We analyze this data with SExtractor (Bertin & Arnouts 1996) excluding all sources that lie close to diffraction spikes around bright stars, adjacent to a small number of remaining cosmetic defects on the final reduced mosaic and within $10''$ of the edge of the field of view. Monte Carlo simulations were used to determine the completeness limits of the J –band catalog. Scaled artificial point–sources that match the seeing were inserted at random positions into the J –band mosaic and examined using the same SExtractor configuration as above. The 80% completeness limit (equivalent to a 5σ detection limit) was determined to be $J(5\sigma) = 21.1$. We then performed aperture photometry for all of the J –detected sources using a 2–arcsec diameter aperture on the seeing matched $BVR IJK$ –band frames. Finally, we removed several hundred stars from the multi–color catalog based on their profile shapes to yield a final catalog of 4376 sources. Using HYPERZ¹⁰ (Bolzonella et al. 2000), we then fitted synthetic spectral templates (Bruzual & Charlot 1998) to all 4376 galaxies in the $BVR IJK$ photometric catalog, adopting a Calzetti et al. (2000) extinction law, and allowing dust extinction in each galaxy to be $A_V \leq 1.2$.

The resulting photometric redshift distribution in Fig. 2 shows that the foreground cluster, C10024 ($z=0.4$), is well recovered in the photometric redshift analysis. The photometric redshift reliability at higher redshifts can be gauged by comparing with the extensive spectroscopic catalog of Moran et al. (2004, in prep. – see also Czoske et al. 2001; Treu et al. 2003). The overlap between the photometric and spectroscopic catalogs is limited beyond $z=1$ because the wavelength coverage of the spectroscopic observations ($\lambda \lesssim 0.75 \mu\text{m}$ – e.g. Treu et al. 2003) was designed to locate cluster members at $z \simeq 0.4$. Nonetheless, in the region of

overlap the mean photometric redshift error is $\langle \Delta_z \rangle = 0.04$, where $\Delta_z \equiv (z_{\text{spec}} - z_{\text{phot}})/(1 + z_{\text{spec}})$. The rms scatter, defined as $\sigma_z^2 \equiv (N-1)^{-1} \Sigma ((\Delta_z - \langle \Delta_z \rangle)/(1 + z_{\text{spec}}))^2$, where N is the number of galaxies, is also small: $\sigma_z = 0.1$.

The final step in constructing the $z \simeq 1$ field sample is to select all galaxies within a suitable redshift range chosen to yield an adequate–sized sample for the field of view. We adopted a range $0.75 \leq z \leq 1.25$. Down to a luminosity $M_V \leq -21.2$ (see §2.1) the combined photometric/spectroscopic catalog yields a sample of 843 galaxies.

Determining the optimal redshift bin, δz , for estimating the galaxy density is a trade–off between two effects. To avoid spurious associations δz should ideally be as small as possible. However, given the use of photometric redshifts, it is pointless making the bin smaller than the typical error in estimated redshift. After some experimenting, at each field galaxy position, the ten nearest neighbors within a redshift slice ($\delta z = \pm 0.1$) centered on the best–fit photometric redshift (or spectroscopic redshift where available) were located. The corresponding area was then computed as described above (§3.1.1). Two corrections were subsequently applied. First, a field correction in each redshift slice was computed by scaling the number of galaxies within the entire field–of–view in each slice. This leads to a reduction in the value of Σ at each location. The second correction takes account of uncertainties in the photometric redshifts. For simplicity we assume that these uncertainties are normally distributed. Since the measured scatter ($\sigma_z(1+z) \simeq 0.2$) is somewhat larger than the width $\delta z = \pm 0.1$ of the interval employed for the density measurement, the local density measurements are underestimated by a factor of ~ 2 . The morphology–density relation is very flat at the densities probed by these data (Fig. 3), therefore this correction for photometric redshift uncertainties has a negligible effect on the final results.

3.2. Morphological Classification

The total number of $z \simeq 1$ galaxies for which detailed morphological information is available is 1257. This comprises all 957 members of the high–density cluster catalog (§3.1.1) and 300 members out of the total of 843 galaxies in the low–density field catalog (§3.1.2) which lie on the sparse–sampled *HST* mosaic of C10024 (§2.2).

Postage stamp images ($5'' \times 5''$) of all 1257 galaxies were extracted and classification was performed using a scheme comprising stellar/compact, early–type (E/S0), late–type (Sa and later) and faint categories, patterned after that employed by Treu et al. (2003) but with broader classes designed to take account of the lower signal–to–noise ratio of the most distant galaxies targeted by this study. One of us (GPS) classified all 1257 galaxies, and a control sample comprising a sub–set of roughly one third of the total sample was cross–classified by three of the authors (GPS, TT, RSE). The majority of the differences in the latter test arose from difficulties in classifying unambiguously bulge dominated galaxies as either E/S0 (i.e. early–types) or Sa (i.e. late–types in our scheme). We use these three independent morphological catalogs to estimate the uncertainty in the early type fraction (6%) and add this in quadrature to the statistical errors when presenting our final results in §4.1.

4. RESULTS

4.1. The Morphology–density Relation at $z=1$

We now combine measurements of projected galaxy number density and the morphological classifications to construct

¹⁰ Available at <http://webast.ast.obs-mip.fr/hyperz>

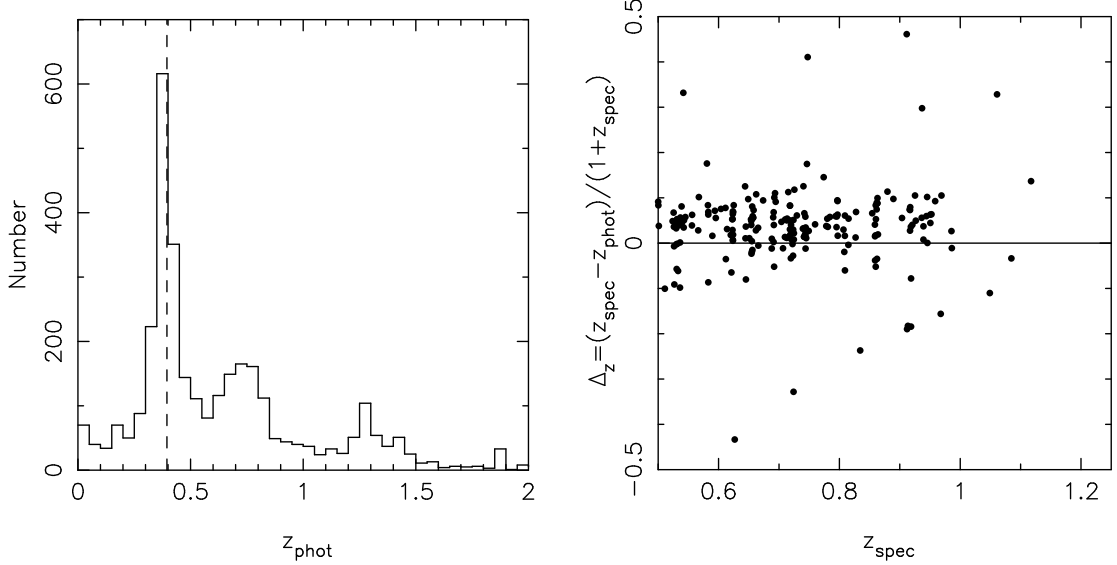


FIG. 2.— LEFT: Photometric redshift distribution in the field of the cluster Cl0024 derived from the spectral template fitting using HYPERZ. The foreground cluster at $z=0.4$ is clearly recovered, in addition to a significant population of galaxies at $0.75 \leq z \leq 1.25$ which forms the basis of this study. RIGHT: Comparison of photometric and spectroscopic redshifts from the catalog of Moran et al. (2004, in prep.). The comparison indicates a mean redshift error of $\langle \Delta_z \rangle = 0.04$ and rms scatter of $\sigma_z = 0.1$. See §3.1.2 for further details.

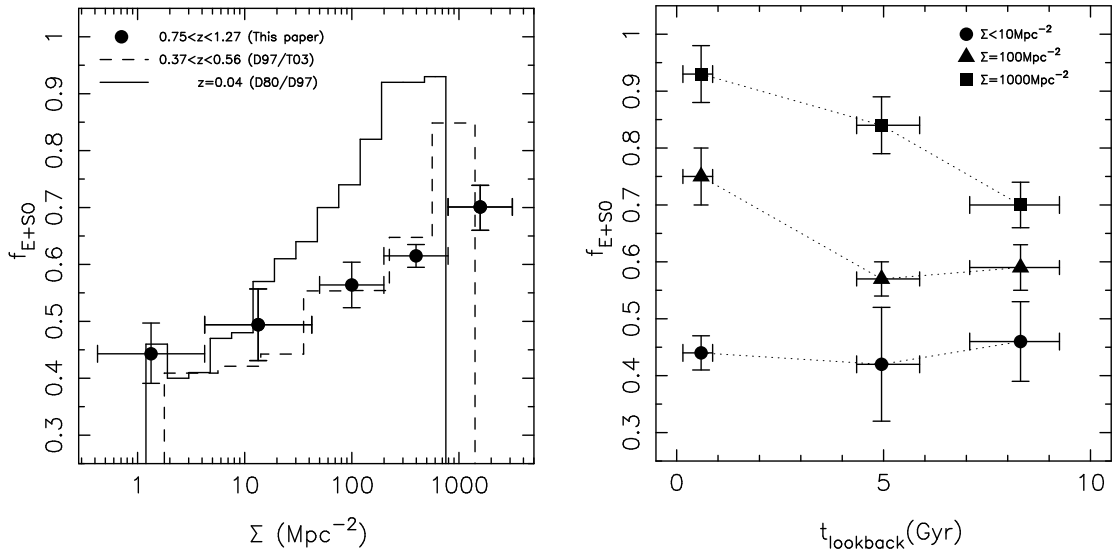


FIG. 3.— LEFT: Early type fraction f_{E+S0} versus projected density at various redshifts. Vertical error bars on the filled data points represent the sum of uncertainties arising from counting statistics, morphological misclassification, photometric redshifts (for the two lowest density points) and field-to-field variance (for the three high-density points). Horizontal error bars define bin widths chosen to contain >100 galaxies. The histograms show the low and intermediate redshift data presented by Dressler et al. (1997); the $z=0.5$ data is rebinned to include the results of Treu et al. (2003) and to achieve a signal-to-noise ratio comparable with the high-redshift data. RIGHT: Evolution of the early-type fraction f_{E+S0} versus look-back time for various projected densities derived from the data presented on the left.

the morphology–density relation at $z=1$ (Fig. 3). For simplicity we summarize this relation in terms of the early-type fraction, f_{E+S0} , as a function of redshift and environmental density.

Our data span three orders of magnitude in projected density from the "field", $\Sigma < 10 \text{ Mpc}^{-2}$, to cluster cores, $\Sigma \simeq 1000 \text{ Mpc}^{-2}$. The three highest density points are derived from the pointed cluster observations (§3.1.1); the two lowest density points are derived from our analysis of the field viewed in the Cl0024 mosaiced image (§3.1.2). Horizontal error bars show bin widths chosen to contain a minimum of

100 galaxies (the $\Sigma = 400 \text{ Mpc}^{-2}$ bin contains in excess of 600 galaxies). Vertical error bars combine binomial uncertainties (Gehrels et al. 1986) with two further contributions added in quadrature. First, we quantify the cluster-to-cluster scatter by recomputing the high density points, each time excluding one of the clusters (see Table 1). The rms scatter between these measurements of f_{E+S0} is ~ 0.03 , i.e. comparable with or smaller than the typical binomial uncertainty. We also include the effect of morphological misclassifications as noted in §3.2.

Fig. 3 clearly shows that morphological segregation was al-

ready present at $z=1$. The early type fraction f_{E+S0} monotonically increases with projected density, Σ . Previous studies of the fraction of early–type galaxies at early times concentrated on individual galaxy clusters (e.g. van Dokkum et al. 2000, 2001; Lubin et al. 2002). These authors found fractions consistent with those presented here when allowance is made for the fact that averages were taken over larger areas (the entire WFPC2 field in most cases) thereby sampling a range of projected densities. Taking MS 1054–0321 as an example, van Dokkum et al. (2000) found $f_{E+S0}=0.5\pm 0.1$ at densities of $\Sigma\approx 50$, which is consistent with the results presented in Fig. 3.

4.2. Evolution of the Morphology–density Relation

Fig. 3 also presents histograms of f_{E+S0} as a function of projected density for the local and intermediate samples, $z\approx 0$ and $z\approx 0.5$. The former is based on Dressler et al.’s (1997) re–analysis of Dressler’s (1980) data. The latter combines Dressler et al.’s (1997) study of the core regions of 10 clusters at $0.37\leq z\leq 0.56$ with Treu et al.’s (2003) panoramic study of Cl 0024 ($z=0.4$). In combining these two datasets, we re–binned Dressler et al.’s data to be consistent with the Treu et al. data and took a simple average in the region where the two datasets overlap, i.e. $\Sigma\geq 30\text{Mpc}^{-2}$.

Although we detect a morphology–density relation at $z=1$, it is not as prominent as in the local universe. We quantify this evolution by fitting a straight–line of the form $f_{E+S0}\propto\beta\log\Sigma$ to both the $z=0$ and $z=1$ data. We obtain $\beta(z=0)=0.26\pm 0.01$ and $\beta(z=1)=0.08\pm 0.02$. The morphology–density relation, as summarized by the early–type fraction, is therefore ~ 3 times steeper locally than at $z=1$.

We also compare our $z\approx 1$ results with those at $z=0.5$, and find, perhaps surprisingly, that there has been little evolution between $z=1$ and $z=0.5$, except in the densest bin, i.e. $\Sigma\approx 1000\text{Mpc}^{-2}$. Fitting our simple model to the $z=0.5$ data, we obtain $\beta(z=0.5)=0.15\pm 0.05$. If we exclude the highest density bin, the result changes only slightly: $\beta(z=0.5)=0.13\pm 0.05$. Both of these values agree within the uncertainties with the slope found at $z=1$.

A simpler way to present our results is the run of f_{E+S0} as a function of look–back time for low ($\Sigma\leq 10\text{Mpc}^{-2}$), intermediate ($\Sigma=100\text{Mpc}^{-2}$), and high ($\Sigma=1000\text{Mpc}^{-2}$) densities (see Fig. 3). This elucidates more clearly the timing of environmental evolution. Little evolution is seen in the early–type fraction in low density environments over $0<z<1$. Evolution at intermediate densities occurred remarkably recently (i.e. in the last 5 Gyr) with little evidence for any change at earlier times. In the highest density regions, there has been a monotonic rise with cosmic times.

5. DISCUSSION

We first consider why the fraction of early–type galaxies increases first in the higher density environments, then in intermediate density environments and finally – if it does at all – in the lowest density environments. Qualitatively, this can be understood in the scenario of hierarchical structure formation. At a given epoch, the densest regions are those which started collapsing earliest; in terms of age since collapse, the densest regions are therefore the oldest. If we assume that the original morphological mix is universal and then late–type galaxies are transformed into early–types by environmental processes, then the densest regions have had more time to increase their early–type fraction. Clearly, the rate of transformation could also be a function of density, for example dense clusters are likely to be more efficient than poor groups at inducing ram–

pressure stripping, and therefore the metamorphosis could be accelerated once some threshold conditions are met. In summary, the broad picture presented by our results is in qualitative agreement with the hierarchical paradigm. We now turn to more quantitative possible explanations for our results. We begin with a brief review of the evolution of early–type galaxies in clusters.

For some years now, evidence spanning the range $0<z<1$ has suggested that cluster early–types represent a very homogeneous, slowly evolving population. This is based in part on the low intrinsic scatter (~ 0.08 mags) observed in the local color–magnitude relation (Bower, Lucey & Ellis 1992) and that tracked to $z\approx 1$ (Ellis et al. 1997; Stanford, Eisenhardt & Dickinson 1998). The mass–to–light ratios deduced from the fundamental plane provide a second indicator, both at low redshift (e.g., Lucey et al. 1991; Pahre, Djorgovski, & de Carvalho 1998) and intermediate redshifts (e.g. van Dokkum & Franx 1996; Bender et al. 1998; van Dokkum et al. 1998; Kelson et al. 2000). Both results have supported the widely–held view that the stars in *some* cluster early–types formed at high redshift (i.e. $z>2$).

This does not necessarily mean that *all* local early–types evolved from those seen at earlier times. Conceivably some formed subsequent to $z\approx 0.5$ –1 but nonetheless found their way onto the present–day fundamental plane and color–magnitude relations (Bower, Terlevich & Kodama 1998). This is particularly likely for the lenticulars which may have been transformed relatively recently from star–forming galaxies (Dressler et al. 1997). However, the physical processes that govern how star–forming disk galaxies are transformed into quiescent lenticulars remains an important outstanding question (e.g. Kodama & Smail 2001; Treu et al. 2003).

Motivated by our new results, we now explore what new clues we can deduce about the evolution of cluster early–type galaxies. Specifically, we use several evolutionary scenarios to attempt to set a limit on the fraction of lenticular galaxies, f_{S0} , in clusters at $z=1$. Note that we restrict our attention to the high density regions; this is because measurements of f_{S0} are not available at lower redshift for the intermediate and low density regimes. The crux of our model is to use our measurement of f_{E+S0} at $z=1$, in combination with the elliptical galaxy fraction, f_E , at $z=0.5$ (Dressler et al. 1997; Treu et al. 2003; §4.2) and simple model assumptions to estimate f_{S0} at $z=1$. We write the following expression for the lenticular fraction at $z=1$:

$$f_{S0,z=1}=f_{E+S0,z=1}-f_{E,z=0.5}\frac{N_{z=0.5}}{N_{z=1}}+\frac{\Delta N_E}{N_{z=1}} \quad (1)$$

We derive Equation 1 from first principles in the Appendix, however it is quite straightforward to understand each term. From the early–type fraction at $z=1$ ($f_{E+S0,z=1}$), we subtract the elliptical fraction at $z=0.5$, re–normalized to account for changes in the total number of galaxies due to evolutionary processes such as in–fall and galaxy–galaxy mergers. We also add a term to account for changes in the number of elliptical galaxies due to these evolutionary processes; we divide the change in the number of ellipticals ($\Delta N_E=N_{E,z=0.5}-N_{E,z=1}$) by the total number of galaxies at $z=1$.

We now employ a series of evolutionary scenarios from which we estimate values of $N_{z=0.5}/N_{z=1}$ and $\Delta N_E/N_{z=1}$, and thus, in combination with measurements of $f_{E+S0,z=1}$ and $f_{E,z=0.5}$ derive estimates of $f_{S0,z=1}$. The numerical details of each scenario are listed in the Appendix.

We first adopt a closed box model in which we assume that all cluster ellipticals are formed at high redshifts, say $z > 2$, and that the rising fraction of early-type galaxies (i.e. ellipticals and lenticulars) with cosmic time arises entirely as a result of lenticulars transformed from star-forming spirals. A key prediction of this model, and indeed the open box models discussed below, is the existence of an epoch at which the early-type galaxy population in clusters is “pristine”, i.e. comprises solely ellipticals formed at high redshift. Any measure of the fraction of lenticular galaxies (f_{S0}) as a function of redshift would then yield important constraints on the timing and the physics of galaxy transformation in clusters.

For the closed box model, at $z \lesssim 1$, ellipticals are neither created nor destroyed ($\Delta N_E = 0$) and there is no overall number evolution ($N_{z=0.5} = N_{z=1}$). The lenticular fraction at $z=1$ is therefore simply the difference between the early-type fraction at $z=1$ ($f_{E+S0, z=1} = 0.7 \pm 0.1$) and the elliptical fraction at $z=0.5$ ($f_{E, z=0.5} = 0.6 \pm 0.1$ – Dressler et al. 1997; Treu et al. 2003). We therefore derive a crude upper limit of $f_{S0, z=1} \lesssim 0.1$. Given the uncertainties in the observational data, in this picture, we could be witnessing such a “pristine” population of cluster ellipticals at $z \simeq 1$. However, clusters are probably not closed boxes; numerical simulations demonstrate that material is continually accreted into clusters, generally along the filamentary structure. We therefore also explore several open box models, with the aim of finding out whether additional evolutionary processes tend to increase or decrease the closed box estimate of $f_{S0, z=1}$.

First, we relax the assumption that there is no in-fall from the field; we retain the assumption that there is no number evolution in the ellipticals ($\Delta N_E = 0$). If we assume that the $z=1$ cluster galaxy population has increased by 20% at $z=0.5$ due to in-fall of spirals and lenticulars, then $N_{z=0.5}/N_{z=1} = 1.2$ and $f_{S0, z=1} \simeq 0$. Note that this scenario includes implicitly the possibility that the in-falling spirals are transformed into lenticulars. This simple in-fall scenario therefore supports the idea that f_{S0} is negligible at $z=1$.

We now consider number evolution in the elliptical galaxies; his could occur through several processes, for example some of the in-falling population could already be ellipticals, spiral and/or lenticulars could merge to form ellipticals either in the cluster core or in the in-falling groups (e.g. van Dokkum et al. 1999) and ellipticals in the cluster cores could merge together to form a brightest cluster galaxy (hereafter BCG; e.g. Nipoti et al. 2003). Taking the possibility of in-falling ellipticals first, we add 10% in-fall of ellipticals to the 20% in-fall of spirals and lenticulars described above: $\Delta N_E/N_{z=1} = 0.1$; $N_{z=0.5}/N_{z=1} = 1.3$. Substituting these values into Equation 1 reveals that this scenario is also consistent with a very low lenticular fraction at $z=1$ – $f_{S0, z=1} \simeq 0.02$.

We now include galaxy-galaxy mergers as a mechanism for generating cluster ellipticals, and for simplicity assume zero in-fall from the field. If ten in every hundred cluster spirals at $z=1$ merge pair-wise to produce half that number of ellipticals by $z=0.5$, then $N_{z=0.5}/N_{z=1} = 0.95$ and $\Delta N_E/N_{z=1} = 0.05$, which translates into $f_{S0, z=1} \simeq 0.2$. Combining this scenario with in-fall of a similar fraction of spiral galaxies to that discussed above modifies the second term in Equation 1 thus: $N_{z=0.5}/N_{z=1} \simeq 1.2$, and the lenticular fraction thus: $f_{S0, z=1} \simeq 0.03$.

Finally, under a galactic cannibalism scenario (e.g. Nipoti et al. 2003), the number of cluster ellipticals reduces with time due to their ingestion into the BCG. If 5 per cent of clus-

ter ellipticals at $z=1$ have been cannibalized by $z=0.5$, then $N_{z=0.5}/N_{z=1} \simeq 0.97$ and $\Delta N_E/N_{z=1} = -0.03$, which translates into $f_{S0, z=1} \simeq 0.09$. Again, adding 20 per cent in-fall of spiral galaxies to a cannibalism scenario yields $N_{z=0.5}/N_{z=1} \simeq 1.17$, and a lenticular fraction of: $f_{S0, z=1} \simeq 0$. This demonstrates that it is unreasonable to assume that the agent of change is only the spiral population and that a combination of cannibalism and in-fall in the open box case can be arranged to yield a low lenticular fraction at $z=1$.

In summary, we have used simple models to explore several scenarios for the evolution of early-type galaxies between $z=1$ and $z=0.5$, with the aim of constraining the fraction of lenticular galaxies in clusters at $z=1$. Whilst the scenarios considered are unlikely to represent an exhaustive study, it is interesting to note that in all except one scenario the lenticular fraction is $f_{S0} = 0.1$ or lower. This is comparable with the uncertainty on the observational data included in the calculations using Equation 1. At $z=1$, we may therefore be observing cluster galaxy populations at or very close to their “pristine” state, in a scenario where the bulk of the elliptical population formed at higher redshifts ($z > 2$).

Our suggestion that the lenticular fraction at $z=1$ is negligible is clearly speculative. Additional data is required to test this interpretation, most importantly, a discriminator between elliptical and lenticular galaxies at high redshift is required. In addition to deep *HST/ACS* imaging for morphologies, resolved spectroscopy of early-type galaxies in clusters at $z \simeq 1$ and beyond should help to discriminate between those galaxies that are dynamically hot (elliptical galaxies) and those that are cold, i.e. lenticular galaxies with systematic rotation. Already, promising exploratory studies have demonstrated the feasibility of making this distinction (van Dokkum & Stanford 2001, Iye et al. 2003).

6. CONCLUSIONS

We have used 52 individual *HST/WFPC2* observations through the F814W filter, supplemented by panoramic ground-based imaging to measure the morphology-density relation of galaxies at $z=1$. Our study adopts analysis methods similar to those developed at lower redshifts (e.g. Dressler 1980) and our principal achievement is to span, at $z \simeq 1$, the full three orders of magnitude range in the projected number density of galaxies encompassed by the low redshifts studies. We choose to make a like-for-like comparison of the early-type fractions spanning field ($\Sigma \lesssim 10 \text{ Mpc}^{-2}$), group ($\Sigma \simeq 100 \text{ Mpc}^{-2}$) and rich cluster ($\Sigma \simeq 1000 \text{ Mpc}^{-2}$) environments.

We briefly summarize our findings as follows:

- (i) Morphological segregation remains a prominent feature of the galaxy population at $z=1$, although the slope of the $f_{E+S0} - \log \Sigma$ relation is ~ 3 times shallower than observed locally.
- (ii) The morphology-density relations at $z=1$ and $z=0.5$ are remarkably similar, with a significant difference only detected in the highest density bin. Most of the evolution producing the locally-observed relation occurred in the redshift interval $0 < z < 0.5$.
- (iii) At low densities, the early-type fraction is roughly constant at $f_{E+S0} = 0.4 \pm 0.1$ across the full redshift range ($0 < z < 1$).

These trends suggest to us a simple model whereby most cluster ellipticals formed at high redshift ($z > 2$) with the bulk of the density–dependent growth arising from the environmental transformation of in–falling disk galaxies into lenticulars, and possibly merging of cluster galaxies at later times. This is motivated by the suggestive agreement (within the uncertainties) between the early–type fraction at $z=1$ in high density regions with the elliptical fraction observed at $z=0.5$. Within the observational uncertainties, the majority of the model scenarios that we have explored are consistent with a negligible lenticular fraction at $z=1$, $f_{S0} \lesssim 0.1$. It is therefore possible that all cluster early–types at $z=1$ are ellipticals. To test this suggestion, resolved dynamical data is needed for a large sample of early–type cluster and field galaxies whose environmental densities can be measured.

ACKNOWLEDGMENTS

GPS thanks Andrew Benson, Pieter van Dokkum and David Sand for helpful discussions and comments. We are grateful to Jean–Paul Kneib and Oliver Czoske for generously sharing their ground–based optical data with us. We thank Kevin Bundy, David Thompson and John Carpenter for helpful comments on the NIR data reduction and calibration, and thank Chris Conselice for assistance with the NIR observations. We also recognize Ian Smail and David Gilbank’s valiant efforts in 2000/2001 to obtain and reduce wide–field NIR imaging data of Cl0024. We acknowledge financial support for proposal HST–GO–8559. TT also acknowledges support from NASA through Hubble Fellowship grant HF–01167.01. Finally, we recognize and acknowledge the cultural role and reverence that the summit of Mauna Kea has within the indigenous Hawaiian community. We are most fortunate to have the opportunity to conduct observations from this mountain.

APPENDIX

DERIVATION OF EQUATION 1

Equation 1 describes how the fraction of lenticular galaxies at $z=1$ ($f_{S0,z=1}$) can be estimated from two observable quantities: the fraction of early–type galaxies at $z=1$ ($f_{E+S0,z=1}$) and the fraction of elliptical galaxies at $z=0.5$ ($f_{E+S0,z=0.5}$). As explained in §5, the equation is quite intuitive, however for completeness, we derive it here from first principals. First, we write the early–type fraction at $z=1$ in terms of the elliptical and lenticular fractions at that redshift:

$$f_{E+S0,z=1} = f_{E,z=1} + f_{S0,z=1} \quad (\text{A1})$$

Simple re–arrangement, where $N_{z=1}$ is the total number of cluster galaxies and $N_{E,z=1}$ is the number of cluster ellipticals, both at $z=1$, gives:

$$f_{S0,z=1} = f_{E+S0,z=1} - \frac{N_{E,z=1}}{N_{z=1}} \quad (\text{A2})$$

We now define $\Delta N_E = N_{E,z=0.5} - N_{E,z=1}$ to be the change in the number of cluster ellipticals between $z=1$ and $z=0.5$, and re–write Equation A2 as:

$$f_{S0,z=1} = f_{E+S0,z=1} - \frac{N_{E,z=0.5} - \Delta N_E}{N_{z=1}} \quad (\text{A3})$$

Finally, we substitute $N_{E,z=0.5} = f_{E,z=0.5} \cdot N_{z=0.5}$, to obtain Equation 1 from §5:

$$f_{S0,z=1} = f_{E+S0,z=1} - f_{E,z=0.5} \frac{N_{z=0.5}}{N_{z=1}} + \frac{\Delta N_E}{N_{z=1}} \quad (\text{A4})$$

TABULATION OF CLOSED AND OPEN BOX MODELS

In this table we list the values used in Equation 1 in §5.

	$f_{S0,z=1} = f_{E+S0,z=1} - f_{E,z=0.5} \cdot N_{z=0.5} / N_{z=1} + \Delta N_E / N_{z=1}$					
Closed Box Model						
[A] No in–fall, no number evolution	$f_{S0,z=1} =$	0.7	–	0.6×1	+	0 = 0.1
Open Box Models						
[B] 20% in–fall of spirals and lenticulars	$f_{S0,z=1} =$	0.7	–	0.6×1.2	+	0 = –0.02
[C] Model B plus 10% in–fall of ellipticals	$f_{S0,z=1} =$	0.7	–	0.6×1.3	+	0.1 = 0.02
[D] 10% of the total population (assumed to be spirals) merge pair–wise to form ellipticals	$f_{S0,z=1} =$	0.7	–	0.6×0.95	+	0.05 = 0.18
[E] Model D plus Model B	$f_{S0,z=1} =$	0.7	–	0.6×1.2	+	0.05 = 0.03
[F] Cannibalism – 5% of ellipticals merge to form a BCG	$f_{S0,z=1} =$	0.7	–	0.6×0.97	–	0.03 = 0.09
[G] Model F plus Model B	$f_{S0,z=1} =$	0.7	–	0.6×1.17	–	0.03 = –0.03

REFERENCES

- Andreon S., 1998, *ApJ*, 501, 533
 Baugh C.M., et al., 1996, *MNRAS*, 283, 1361
 Balogh M.L., Smail I., Bower R.G., Ziegler B.L., Smith G.P., Davies R.L., Gaztelu A., Kneib J.-P., Ebeling H., 2002, *ApJ*, 566, 123
 Bender R., Saglia R.P., Ziegler B., Belloni P., Greggio L., Hopp U., Bruzual G., 1998, *ApJ*, 493, 529
 Benson A.J., et al., 2001, *MNRAS*, 327, 1041
 Bertin, Arnouts, 1996, *A&AS*, 117, 393
 Bolzonella M., Miralles J.-M., Pelló R., 2000, *A&A*, 363, 476
 Bower R.G., Lucey J.R., Ellis R.S., 1992, *MNRAS*, 254, 601
 Bower R.G., Kodama T., Terlevich A. 1998, *MNRAS* 299, 1193
 Brown W.R., Geller M.J., Fabricant D.G., Kurtz M.J., 2001, *AJ*, 122, 714
 Bruzual A.G., Charlot S., 1993, *ApJ*, 405, 538
 Calzetti D., Armus L., Bohlin R.C., Kinney A.L., Koornneef J., Storchi-Bergmann T., 2000, *ApJ*, 533, 682
 Chen H., Marzke R.O., McCarthy P.J., Martini P., Carlberg R.G., Persson S.E., Bunker A., Bridge C.R., Abraham R.G., 2003, *ApJ*, 586, 745
 Coleman G.D., Wu C.-C., Weedman D.W., 1980, *ApJS*, 43, 393
 Couch W.J., Barger A.J., Smail I., Ellis R.S., Sharples R.M., *ApJ*, 497, 188
 Cuillandre J.-C. et al. 2000, in *Optical and IR Telescope Instrumentation and Detectors*, eds. Iye M. & Moorwood A., S.P.I.E., 4008, 1010.
 Czoske O., Kneib J.-P., Soucail G., Bridges T.J., Mellier Y., Cuillandre J.-C., 2001, *A&A*, 372, 391
 Czoske O., 2002, PhD Thesis, Observatoire Midi-Pyrénées, Université Paul Sabatier, Toulouse, France
 Davis M., et al., 2002, *Proc. SPIE*, 4834, 161 (astro-ph/0209419)
 Diaferio A., Kauffmann G., Balogh M.L., White S.D.M., Schade D., Ellingson E., 2001, *MNRAS*, 323, 999
 Dressler A., 1980, *ApJ*, 236, 351
 Dressler A., et al., 1997, *ApJ*, 490, 577
 Ellis R.S., Smail I., Dressler A., Couch W.J., Oemler A., Butcher H., Sharples R.M., 1997, *ApJ*, 483, 582
 Fabricant D., Franx M., van Dokkum P., 2000, 539, 577
 Fasano G., Poggianti B.M., Couch W.J., Bettoni D., Kjaergaard P., Moles M., 2000, *ApJ*, 542, 673
 Frenk C.S., White S.D.M., Efstathiou G., Davis M., 1985, *Nature*, 317, 595
 Frenk C.S., White S.D.M., Davis M., Efstathiou G., 1988, *ApJ*, 327, 507
 Gehrels N., 1986, *ApJ*, 303, 336
 Gladders M.D., Yee H.K.C., Ellingson E., 2002, *AJ*, 123, 1
 Helsdon S.F., Ponman T.J., 2003, *MNRAS*, 339, L29
 Hubble E.P., 1926, *ApJ*, 64, 321
 Iye M., Shimasaku K., Miyazaki S., Simpson C., Imanishi M., Kashikawa N., Kodama T., Chiba M., Saito Y., Goto M., et al., 2003, *ApJ*, 590, 770
 Kauffmann G., 1995, *MNRAS*, *MNRAS*, 274, 161
 Kelson D.D., Illingworth G.D., van Dokkum P.G., Franx M., 2000, *ApJ*, 531, 137
 Kneib J.-P., Hudelot P., Ellis R.S., Treu T., Smith G.P., Marshall P., Czoske O., Smail I., Natarajan P., 2003, *ApJ*, 598, 804
 Kodama T., Smail I., 2001, *MNRAS*, 326, 637
 Le Fèvre O., et al., 2003, *A&A*, submitted, astro-ph/0306252
 Lubin L.M., Oke J.B., Postman M., 2002, *AJ*, 124, 1905
 Lucey J.R., Bower R.G., Ellis R.S., 1991, *MNRAS*, 249, 755
 Melnick, Sargent W., 1977, *ApJ*, 215, 401
 Norberg P., et al., 2002, *MNRAS*, 336, 907
 Oemler A., 1974, *ApJ*, 194, 1
 Poli F., Giallongo E., Fontana A., Menci N., Zamorani G., Nonino M., Saracco P., Vanzella E., Donnarumma I., Salimbeni S., et al., 2003, *ApJ*, 593, L1
 Pahre M.A., de Carvalho R.R., Djorgovski S.G., 1998, *AJ*, 116, 1606
 Postman M., Geller M.J., 1984, *ApJ*, 281, 95
 Postman M., Lauer T.R., Szapudi I., Oegerle W., 1998, *ApJ*, 506, 33
 Postman M., Lubin L.M., Oke J.B., 2001, *AJ*, 122, 1125
 Smail I., Ellis R.S., Dressler A., Couch W.J., Oemler A., Sharples R.M., Butcher H., 1997, *ApJ*, 479, 70
 Stanford S.A., Eisenhardt P.R., Dickinson M., 1998, *ApJ*, 492, 461
 Treu T., Stiavelli M., Bertin G., Casertano S., Moller P., 2001, *MNRAS*, 326, 237
 Treu T., Ellis R.S., Kneib J.-P., Dressler A., Smail I., Czoske O., Oemler A., Natarajan P., 2003, *ApJ*, 591, 53
 van Dokkum P.G., Franx M., 1996, *MNRAS*, 281, 985
 van Dokkum P.G., Franx M., Fabricant D., Illingworth G.D., Kelson D.D., 2000, *ApJ*, 541, 95
 van Dokkum P.G., Stanford S.A., Holden B.P., Eisenhardt P.R., Dickinson M., Elston R., 2001, *ApJ*, 552, L101
 van Dokkum P.G., Franx M., 2001, *ApJ*, 553, 90
 van Dokkum P.G. & Stanford, A. 2001 *ApJ* 562, L35
 Wilson J.C., Eikenberry S.S., Henderson C.P., Hayward T.L., Carson J.C., Pirger B., Barry D.J., Brandl B., Houck J.R., Fitzgerald G.J., Stolberg T.M., S.P.I.E. Proc. August 2002